current. The bond weakening at the Mo–C bond may precede because the observed thermal stability is very strongly dependent on not only the α but also β substituents on the alkyl.

In summary, the stereochemistry of the present stoichiometric hydrogenation is comprised of cis insertion and stereoretentive alkane elimination. A four-center transition state is probable for the insertion which implies concertedness. When participation of d orbitals occurs in the process, thermal forbiddenness of a concerted four-center ($_{\sigma}2_s + {}_{\pi}2_s$) reaction is loosened. Similar forbiddenness of the observed stereoretentive three-center alkane elimination is also loosened by d-orbital participation. Then overall cis hydrogenation of olefins is one of the important consequence of bonding through d orbitals.

Acknowledgments. The authors express their acknowledgment for experimental assistance to Mr. J. Izawa, Mr. Y. Terawaki, and Mr. H. Okuda in some preparative works and spectral measurements. We also thank Professor T. Fueno and Dr. O. Kazimoto for the computer programs.

Stereochemical Rigidity in ML_5 Complexes. I. A Detailed Line-Shape Analysis for $Rh[P(OCH_3)_3]_5^+B(C_6H_5)_4^-$ and Other Rhodium(I) Complexes

P. Meakin* and J. P. Jesson

Contribution No. 2047 from the Central Research Department, E. I. du Pont de Nemours & Company, Experimental Station, Wilmington, Delaware 19898. *Received June 22, 1973*

Abstract: The temperature-dependent nmr spectra for several complexes of the type $RhL_5^+X^-$ where L is a phosphite and X^- is a noncoordinating anion are reported. The low-temperature limit proton noise decoupled ^{31}P nmr spectra can be analyzed using an A_2B_3X model indicating that these complexes have D_{3h} symmetry on the nmr time scale at low temperatures. As the temperature is raised, the spectra broaden and coalesce into a symmetric doublet (A part of an A_5X spectrum). The maintenance of ^{31}P–^{103}Rh coupling in the high-temperature limit indicates that this process is intramolecular. At still higher temperatures (above 0°) the spectra again broaden and eventually coalesce into a single line. The higher temperature process involves loss of the ^{103}Rh–^{31}P coupling indicating an intermolecular exchange. A complete density matrix line-shape analysis has been carried out to simulate the temperature-dependent $^{31}P\{^1H\}$ nmr spectra for the intramolecular case. The most detailed analysis has been carried out for the complex $Rh[P(OCH_3)_3]_5^+B(C_6H_5)_4^-$ where a comparison of the observed line shapes with those calculated assuming both simultaneous exchange of the two axial ligands with two of the equatorial ligands and single axial–equatorial exchanges indicates that the simultaneous exchange process dominates. The barriers to the intramolecular mutual exchange process are observed to increase with ligand size and cover the range 7.5–12 kcal/mol. The invariance of the exchange rates to concentration and nature of the anion demonstrates that the barrier height is a property of the cation alone and is not strongly influenced by ion-pairing effects.

In two recent communications,[1,2] we have presented nmr evidence for stereochemical rigidity in a class of five-coordinate d^8 transition metal complexes of the type $ML_5^+X^-$ (M = Co, Rh, Ir) and $ML_5^{2+}(X^-)_2$ (M = Ni, Pd, Pt), with X representing a variety of noncoordinating anions. All previous nmr investigations have indicated that the barriers to intramolecular rearrangement in ML_5 complexes are very low (<5 kcal/mol) resulting in a rapid exchange of the five ligands (on the nmr time scale) at all temperatures attainable in solution.

Earlier studies have included complexes which are isoelectronic with those discussed in the present paper. A single resonance was observed for the natural abundance ^{13}C nmr spectrum of $Fe(CO)_5$ at room temperature.[3] No change was observed in this spectrum on cooling a solution in ether.[4] We have observed that the ^{13}C nmr spectrum of a solution of $Fe(CO)_5$ in 90% chlorodifluoromethane–10% methylene chloride remains a sharp single line down to *ca.* −170°. The ^{19}F nmr spectra of $Fe(PF_3)_5$, $Ru(PF_3)_5$, and $Os(PF_3)_5$ have been recorded down to −160° in chlorodifluoromethane; again, all five ligands were observed to be equivalent on the nmr time scale.[5] More recently, we have recorded the ^{31}P nmr spectra of $Fe(PF_3)_5$ and $Ru(PF_3)_5$ over a similar temperature range in the same solvent; there is no evidence for a slowing down of the exchange process to a rate comparable with the nmr time scale.

It has been widely assumed, without direct experimental evidence, that the Berry process[6] is the most probable rearrangement mechanism in ML_5 systems. The nmr line-shape analysis of Whitesides and Mitchell[7] for $(CH_3)_2NPF_4$ does establish a process involving

(1) J. P. Jesson and P. Meakin, *J. Amer. Chem. Soc.*, **95**, 1344 (1973).
(2) J. P. Jesson and P. Meakin, *Inorg. Nucl. Chem. Lett.*, in press.
(3) F. A. Cotton, A. Danti, J. S. Waugh, and R. W. Fessenden, *J. Chem. Phys.*, **29**, 1427 (1958).
(4) R. Bramley, B. M. Figgis and R. S. Nyholm, *Trans. Faraday Soc.*, **58**, 1893 (1962).
(5) P. Meakin, E. L. Muetterties, and J. P. Jesson, *J. Amer. Chem. Soc.*, **94**, 5271 (1972).
(6) R. S. Berry, *J. Chem. Phys.*, **32**, 933 (1960).
(7) G. M. Whitesides and H. L. Mitchell, *J. Amer. Chem. Soc.*, **91**, 5384 (1969).

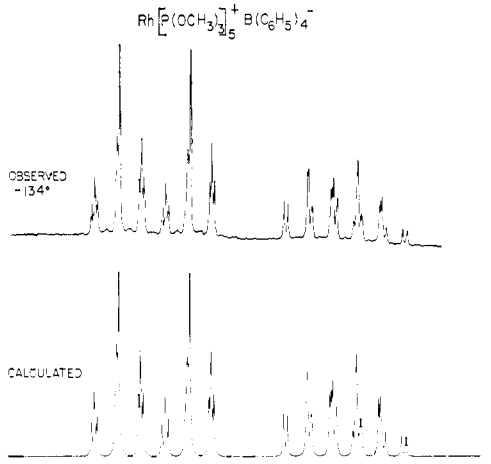

Figure 1. Observed and simulated low-temperature limit (−134°) Fourier mode proton noise decoupled 36.43-MHz ^{31}P nmr spectrum assigned to $Rh[P(OCH_3)_3]_5^+B(C_6H_5)_4^-$ in 90% $CHClF_2$–10% CH_2Cl_2. The simulated spectrum was obtained using an A_2B_3X model with the nmr parameters given in the text.

simultaneous exchange of the axial ligands with a pair of equatorial ligands for this molecule. This is the permutational behavior required by the Berry process and therefore provides strong, indirect, evidence for a similar process in ML_5 complexes. Recent theoretical studies[8] have also provided further support for the Berry mechanism.

In this paper we describe a detailed density matrix analysis of the temperature-dependent nmr line shapes observed in the proton noise decoupled ^{31}P nmr spectrum of $Rh[P(OCH_3)_3]_5^+B(C_6H_5)_4^-$. These calculations show conclusively that the rearrangement involves a simultaneous exchange of the axial ligands with two of the equatorial ligands as required by the Berry process[6] or the turnstile mechanism.[9] Additionally, the temperature-dependent nmr spectra for some other $RhL_5^+X^-$ species are presented.

Studies over a range of concentrations and with different counter ions indicate that ion-pairing effects are unimportant in determining the barrier to, or the nature of, the exchange process.

Subsequent papers in this series will be concerned with the description and analysis of the temperature-dependent nmr spectra of analogous Co(I), Ir(I), Ni(II), Pd(II), and Pt(II) complexes, the synthesis, chemical properties, and intermolecular exchange behavior of these systems, and X-ray crystal studies of some of these complexes.

Two useful approximations for obtaining mechanistic information from temperature-dependent nmr line shapes in complex spectra are described in the Appendix using calculations on the spectra of $Rh[P(OCH_3)_3]_5^+B(C_6H_5)_4^-$ as examples.

Experimental Section

The complexes were prepared by the reaction of excess ligand with $[(C_2H_4)_2RhCl]_2$ in alcoholic solution followed by precipitation with the appropriate counter ion, a procedure similar to that described by Haines.[10] In some cases the complexes were prepared *in situ* in nmr tubes using dichloromethane or acetonitrile as the solvent.

Nmr samples were prepared in a N_2 atmosphere (Vacuum Atmospheres Dri Lab; less than 2 ppm O_2) using deoxygenated solvents where possible. Variable-temperature proton noise decoupled ^{31}P and ^{13}C spectra were recorded in 10-mm sample tubes in the Fourier mode at 36.43 and 22.62 MHz, respectively, using a Bruker HFX 90 with a Digilab FTS/NMR-3 data system and pulser. In those cases where chlorodifluoromethane was used as a solvent, the proton noise decoupled ^{19}F resonance of the solvent was used for field frequency stabilization with a Bruker time-shared ^{19}F lock system. In other solvents 3-mm capillaries containing 1,2-dibromotetrafluoroethane or C_6F_6 were used. Proton spectra were recorded in the time-shared mode in 5-mm sample tubes again using the Bruker spectrometer. In all cases the temperatures were measured by means of a copper–constantan thermocouple located just beneath the sample tube and were calibrated using a similar thermocouple held coaxially in the spinning sample tube partially filled with solvent.

The nmr line-shape calculations were carried out using the density matrix method of Kaplan[11] and Alexander.[12] Details of the mathematical treatment are given in ref 13 and in the Appendix.

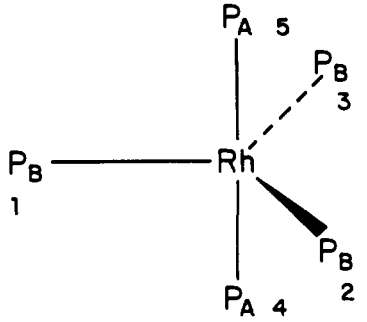

Figure 2. Nuclear labeling scheme for the D_{3h} trigonal bipyramidal ML_5^+ cations.

A. The Temperature-Dependent $^{31}P\{^1H\}$ Nmr Spectra of $Rh[P(OCH_3)_3]_5^+B(C_6H_5)_4^-$

The low-temperature limit proton noise decoupled Fourier mode ^{31}P nmr spectrum of $Rh[P(OCH_3)_3]_5^+B(C_6H_5)_4^-$ was shown in Figure 1 of ref 1 together with a computer simulation. Figure 1 of the present paper shows a much better resolved recording of the same spectrum; we have found that achieving good field homogeneity at low temperature is much easier with the fluorine than with the deuterium lock since quadrupolar broadening of the deuterium resonances becomes excessive at low temperatures (−130 to −160°). The computer simulation in Figure 1 is for an A_2B_3X model using the nmr parameters $|J_{P_AP_B}| = 68$ Hz, $|J_{P_ARh}| = 143$ Hz, $|J_{P_BRh}| = 206$ Hz, and $\delta_{P_AP_B} = 14.5$ ppm (the chemical shift assigned to the A spins is upfield from the shift assigned to the B spins). The good fit obtained between the observed and calculated spectra indicates that the cation has a D_{3h} trigonal bipyramidal structure (Figure 2). The chemical shift difference between the two phosphorus sites is strongly temperature dependent and the samples (using the large 10-mm sample tubes) must be given about 10 min to attain thermal equilibrium in the nmr probe if well-resolved spectra are to be obtained.

To first order, the low-temperature limit spectrum is a doublet of triplets plus a doublet of quartets; how-

(8) R. Hoffmann, J. M. Howell, and E. L. Muetterties, *J. Amer. Chem. Soc.*, **94**, 3047 (1972).
(9) P. Gillespie, P. Hoffman, H. Klusacek, D. Marguarding, S. Pfohl, F. Ramirez, E. A. Tsolis, and I. Ugi, *Angew. Chem., Int. Ed. Engl.*, **10**, 687 (1971), and references therein.
(10) L. M. Haines, *Inorg. Chem.*, **10**, 1685 (1971).
(11) J. I. Kaplan, *J. Chem. Phys.*, **28**, 278 (1958); **29**, 462 (1958).
(12) S. Alexander, *J. Chem. Phys.*, **37**, 967, 974 (1962); **38**, 1787 (1963); **40**, 2741 (1964).
(13) P. Meakin, E. L. Muetterties, F. N. Tebbe, and J. P. Jesson, *J. Amer. Chem. Soc.*, **93**, 4701 (1971).

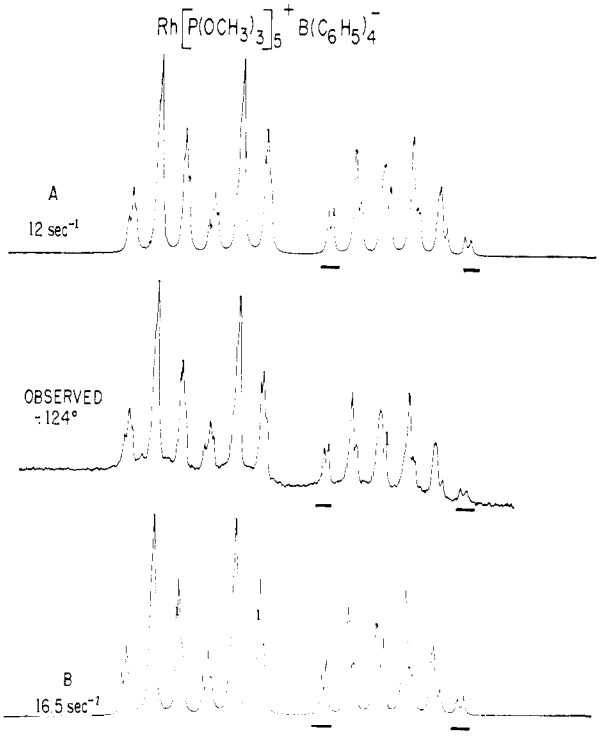

Figure 3. The proton noise decoupled ^{31}P Fourier mode spectrum of $Rh[P(OCH_3)_3]_5^+B(C_6H_5)_4^-$ at $-124°$ in 10% CH_2Cl_2–90% $CHClF_2$, together with spectra simulated for the two permutational mechanisms A and B defined in the text. The appropriate exchange rates are given for the calculated spectra. It is clear that permutational mechanism A which corresponds to simultaneous exchange of the axial ligands with two equatorial ligands gives the better fit.

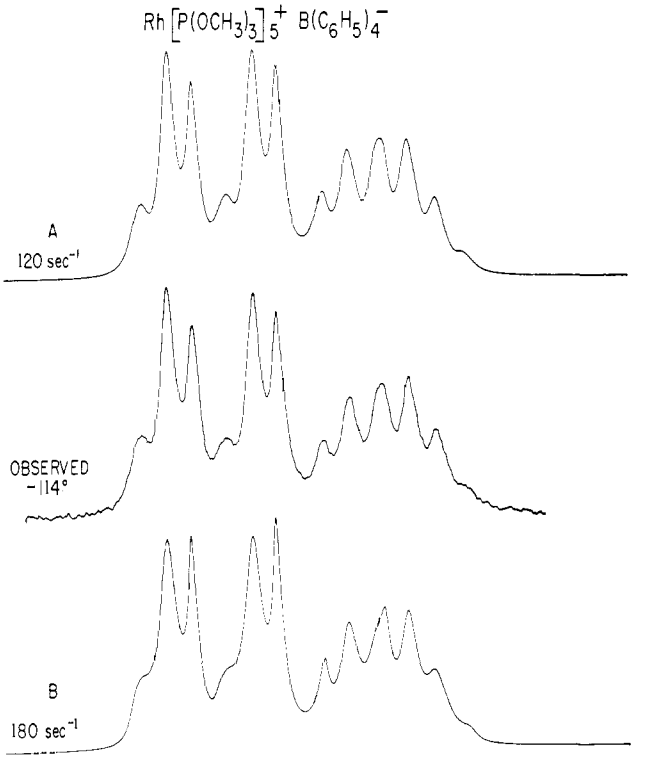

Figure 4. Observed and calculated temperature-dependent proton noise decoupled ^{31}P Fourier mode nmr spectra for a solution of $Rh[P(OCH_3)_3]_5^+B(C_6H_5)_4^-$ in 10% CH_2Cl_2–90% $CHClF_2$ at $-114°$. The permutational mechanisms and exchange rates are given with the calculated spectra in the figure. Permutational mechanism A which corresponds to simultaneous exchange of the axial ligands with two equatorial ligands clearly gives the better fit.

ever, significant higher order effects can be seen and these are accurately reproduced in the calculated spectra (Figure 1). As the temperature is raised, the chemical shift separation decreases and the lines begin to broaden indicating the onset of an exchange process (Figures 3–5). The coupling constants are essentially temperature independent. On further raising the temperature the spectrum becomes very broad and, eventually, in the high-temperature (fast-exchange) limit, coalesces into a sharp doublet with a coupling constant of 180 Hz (Figure 6). This is equal to the weighted average of the low-temperature limit ^{31}P–^{103}Rh coupling constants, and the maintenance of phosphorus–rhodium coupling at high temperatures indicates that the exchange process is intramolecular.

The proton noise decoupled ^{31}P nmr spectrum of $Rh[P(OCH_3)_3]_5^+B(C_6H_5)_4^-$ in acetonitrile at $-40°$ is a doublet with an averaged ^{31}P–^{103}Rh coupling constant of 182 Hz. As the temperature is raised, the doublet begins to broaden and eventually collapses into a single line (Figure 7). An analysis of these intermolecular line-shape effects, with and without added ligand, together with an analysis of the temperature-dependent line-shape effects in the four-coordinate system $Rh[P(OCH_3)_3]_4^+B(C_6H_5)_4^-$ in the presence of 0–1 equiv of added $P(OCH_3)_3$ will be presented in a future paper in this series. It seems clear that the process responsible for the observed line-shape effects in the temperature range 0–100° involves ligand dissociation (eq 1) possibly with competing solvent coordination.

$$RhL_5^+ \rightleftharpoons RhL_4^+ + L \qquad (1)$$

B. Mechanistic Analysis and Line-Shape Calculations

We have recently discussed the possible permutational mechanistic distinctions for mutual exchange in five coordination.[14] For a D_{3h} ML_5 system there are two possible types of temperature-dependent nmr line shapes (three basic permutational sets[13] including the identity). Examples of the two basic permutational sets (excluding the identity) using the labeling in Figure 2 are shown in Table I. Permutational sets of the type A correspond to processes involving simultaneous exchange of the axial ligands (P_4 and P_5) with two of the equatorial ligands (P_1, P_2, and P_3), such as the Berry process; permutational sets of the type B correspond to processes involving single axial–equatorial exchanges.

Table I

Set A	Set B
(15)(24)	(15)(23)
(14)(35)	(12)(35)
(14)(25)	(14)(23)
(25)(34)	(13)(24)
(15)(34)	(13)(25)
(24)(35)	(12)(34)

One of the difficulties encountered in a complete line-shape analysis of the $^{31}P\{^1H\}$ spectra associated with $Rh[P(OCH_3)_3]_5^+B(C_6H_5)_4^-$ is the strong temper-

(14) P. Meakin, E. L. Muetterties, and J. P. Jesson, *J. Amer. Chem. Soc.*, **94**, 5271 (1972).

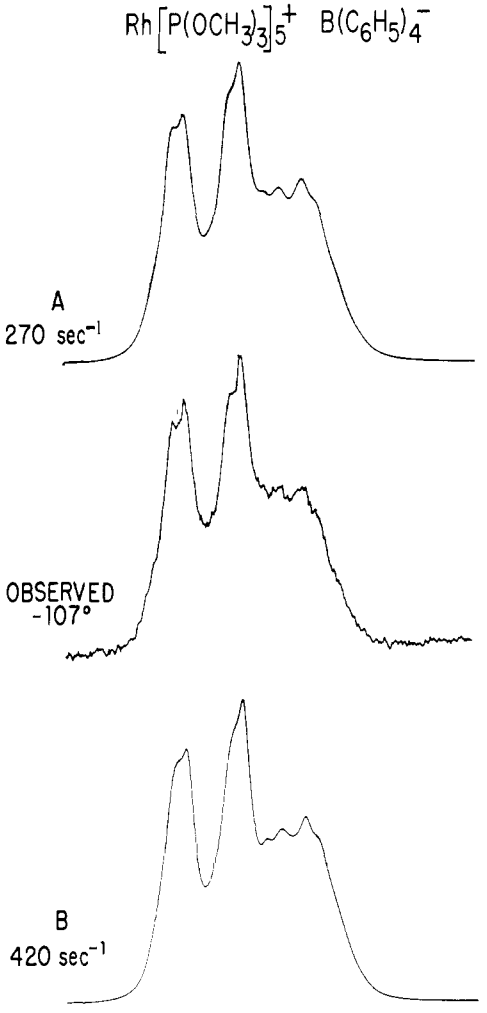

Figure 5. Observed and calculated $^{31}P\{^1H\}$ nmr spectra of a solution of $Rh[P(OCH_3)_3]_5^+B(C_6H_5)_4^-$ in 10% CH_2Cl_2–90% $CHClF_2$ at −107°. The labels A and B identify the basic permutational set used in the line-shape calculations. They are defined in the text.

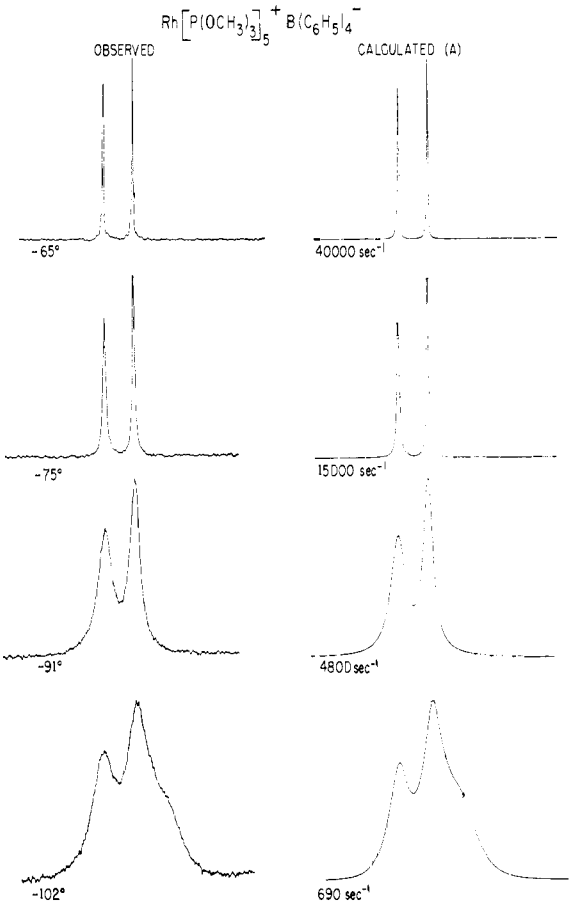

Figure 6. Observed and simulated proton noise decoupled Fourier mode ^{31}P nmr spectra of a solution of $Rh[P(OCH_3)_3]_5^+B(C_6H_5)_4^-$ in 10% CH_2Cl_2–90% $CHClF_2$ at several temperatures (exchange rates). The basic set A was used in the line-shape calculations. In contrast to the spectra obtained at lower temperatures (slower exchange rates), no useful mechanistic information is contained in the details of these line shapes.

ature dependence of the P_A–P_B chemical shift separation. Figure 8 shows this shift separation plotted as a function of temperature together with a somewhat arbitrary extrapolation into the temperature region where the exchange process is too rapid for the shift separation to be measured directly. This extrapolation was used in the line-shape analysis described below. The form of this temperature dependence suggests that it results from a distribution between two or more closely spaced vibrational levels or between two or more distorted structures with zero point energies differing by ~200 cal mol^{-1}. Possible distortions from idealized D_{3h} geometry could arise from steric crowding and the resulting ligand–ligand repulsion interactions.

The middle row of Figure 3 shows the observed spectrum at −124°. The best visual fits obtained using basic permutational sets A and B are shown at the top and bottom of the figure, respectively. The spectra simulated using both basic sets give reasonable fits. However, in matters of detail, that simulated for basic set A is clearly in better agreement with the observed spectrum than that simulated for set B, particularly with respect to the two outer doublets associated with the portion of the spectrum assigned to the axial phosphorus nuclei. These two features, which are underlined in Figure 3, are important because they are the only well-resolved lines in the spectrum. In Figure 4 a similar comparison is made between the observed and calculated spectra at a somewhat higher temperature (exchange rate). Again the best fit is obtained using the basic set A. It should be noted that in this case the major differences between the two simulations occur in the region assigned to the equatorial phosphorus nuclei and do not depend solely on the two features discussed in connection with Figure 3. In Figure 5 a comparison is made between the calculated best fits for sets A and B and the observed spectrum at −107°. Here the difference between the two simulated spectra is less distinct than in Figure 4. Only the central portions of the simulated spectra differ noticeably, but again set A gives the better fit. Above −100°, simulations using the two basic sets become virtually indistinguishable, set B giving the same results as set A at twice the exchange rate used for set A. Figure 6 shows the observed and calculated spectra (using set A) at higher temperatures. The chemical shift separations used in obtaining the simulated spectra shown in Figure 6 were taken from the extrapolation shown in Figure 8. The rate information obtained from the fits obtained in Figure 3–6 for the basic set A is shown in the form of an Arrhenius plot in Figure 9 together with data obtained from spectra at other tem-

Figure 7. Temperature dependence of the proton noise decoupled ^{31}P Fourier mode nmr spectra of a solution of $Rh[P(OCH_3)_3]_5^+B(C_6H_5)_4^-$ in CH_3CN.

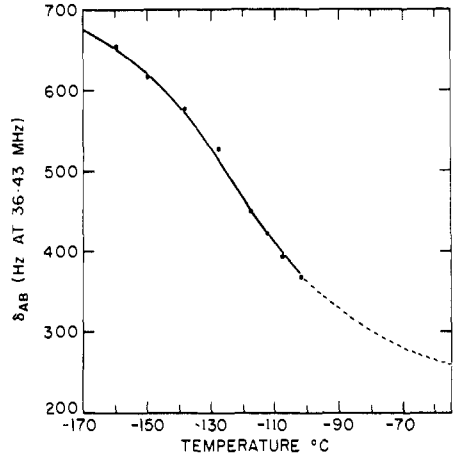

Figure 8. Temperature dependence of δ_{AB} in the proton noise decoupled ^{31}P spectrum of $Rh[P(OCH_3)_3]_5^+B(C_6H_5)_4^-$ in 10% CH_2Cl_2–90% $CHClF_2$. The extrapolation indicated by the dotted line in this figure was used in the line-shape analysis at fast and intermediate exchange rates.

peratures (exchange rates) not illustrated. The straight line in Figure 9 corresponds to the rate expression

$$\text{rate}(T) = 10^{11.8}e^{-6700/RT}$$

or in terms of the Eyring equation $\Delta G^{\ddagger}_{200} = 7.5$ kcal mol^{-1}, $\Delta H^{\ddagger}_{200} = 6.35$ kcal mol^{-1}, and $\Delta S^{\ddagger}_{200} = -5.9$ kcal mol^{-1} deg^{-1}.

The entropy of activation is quite small, consistent with a simple intramolecular process such as the Berry

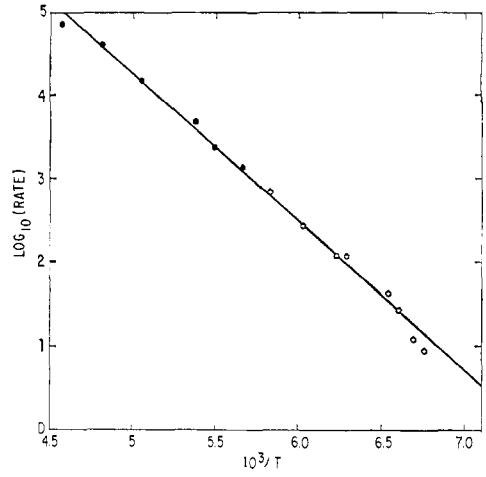

Figure 9. Arrhenius plot obtained from the nmr line-shape analysis of the proton noise decoupled ^{31}P nmr spectra assigned to $Rh[P(OCH_3)_3]_5^+B(C_6H_5)_4^-$. The points represented by filled circles depend on the extrapolation of the chemical shift separation shown in Figure 8.

rearrangement. It should be noted, however, that these results do depend on the chemical shift difference extrapolation shown in Figure 8; only the points represented by open circles in Figure 9 are independent of this extrapolation. They were established by varying the exchange rate and the chemical shift separation to give the best fit between calculated and observed spectra. In contrast, the points represented by the filled circles were obtained by taking the shift separation from the extrapolation and varying the exchange rate only. If a linear extrapolation had been used to estimate the chemical shift separation at higher temperature, the values would be smaller than those actually used; consequently the exchange rates obtained would also be smaller, resulting in a smaller $\Delta H^{\ddagger}$ and a larger (negative) $\Delta S^{\ddagger}$.

C. Concentration Studies

To eliminate the possibility that the temperature dependence of the chemical shift difference for the two phosphorus environments arises from an ion-pairing equilibrium, the concentration dependence of the proton decoupled ^{31}P nmr spectra was investigated. Four solutions in chlorodifluoromethane were examined with concentrations of 0.026, 0.054, 0.12, and 0.23 mol/l. The chemical shift separation was observed to increase with decreasing concentration at several different temperatures (−144, −138, −127, −118, −108, −72, −60°). At the four lower temperatures, the shift separation at 36.4 MHz changed by ~10 Hz (~3%) for an eightfold change in concentration. Although this is a significant shift variation, the same change can be brought about by raising and lowering the temperature only 5° in this temperature range. Since the shift difference is very much more sensitive to temperature than to concentration changes, we conclude that the large temperature effect cannot be explained by an ion-pairing equilibrium. (An eightfold concentration change should have a much larger effect on the degree of dissociation than a 5° temperature change.) Finally, there is no evidence for a variation in exchange rate with concentration at any of the four

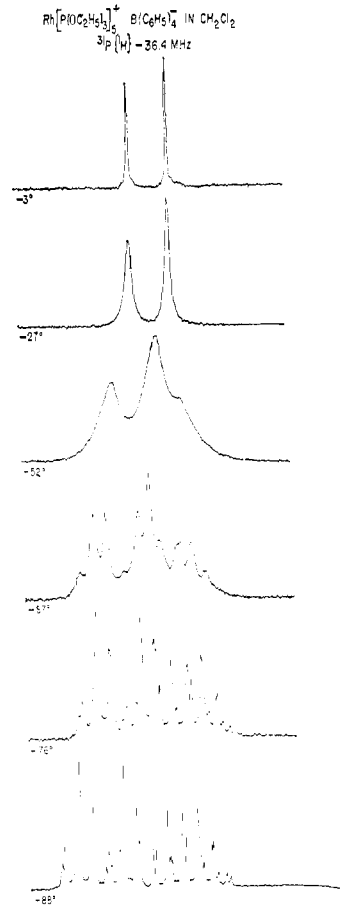

Figure 10. Temperature dependence of the proton noise decoupled 36.43-MHz Fourier mode ^{31}P nmr spectrum of a solution of $Rh[P(OC_2H_5)_3]_5^+B(C_6H_5)_4^-$ in CH_2Cl_2.

higher temperatures showing that there can be no significant contribution to $\Delta G^{\pm}$ from ion-pairing effects.

D. Variation of the Anions

The proton decoupled ^{31}P nmr spectra of the complexes $Rh[P(OCH_3)_3]_5^+X^-$ ($X = B(C_6H_5)_4^-$, $^1/_2GeF_6^{2-}$, $^1/_2SiF_6^{2-}$, PF_6^-, AsF_6^-, SbF_6^-) in 85% $CHClF_2$–15% CH_2Cl_2 were compared at several temperatures in the range −140 to −65°. In all cases there was no significant change in either the exchange rate or the chemical shift separation on changing the anion. For $X^- = B(C_6H_5)_4^-$ the purified complex was used, and in the remaining cases the complexes were prepared in CH_2Cl_2 solution at room temperature by the reaction of $[(C_2H_4)_2RhCl]_2$ with trimethyl phosphite and an appropriate salt of the anion. When the reaction was complete, $CHClF_2$ was added at Dry Ice temperatures, and the complexes were studied without isolation. The salts used in these *in situ* preparations were $KSbF_6$, $(NH_4)_2GeF_6$, $(NH_4)_2SiF_6$, NH_4PF_6, and $KAsF_6$.

The insensitivity of the six sets of spectra to variation of the anion is additional evidence that the observed temperature-dependent nmr spectra are determined by properties of the isolated cation and that ion-pairing effects are not involved.

E. ^1H and ^{13}C Nmr Spectra

The ^1H and ^{13}C nmr spectra for $Rh[P(OCH_3)_3]_5^+B(C_6H_5)_4^-$ have been recorded over the same temperature range as the ^{31}P spectra. At the low-temperature limit the proton decoupled ^{13}C spectrum consists of two single lines with intensity ratio ~2:3 as expected from the structure shown in Figure 2. At −135° the resonance assigned to the ^{13}C nuclei of the equatorial ligands lies 3.25 ppm to low field of that assigned to the ^{13}C nuclei associated with the axial ligands. (The averaged ^{13}C shift is ~45 ppm down-field from TMS.) As the temperature is raised, the spectrum broadens and then coalesces into a sharp single line. These line shapes contain no mechanistic information since the spectral changes are too simple. The ^1H nmr spectrum is also temperature dependent over this range of temperatures, and, in contrast to the ^{13}C spectra, in this case the data are too complex to be useful in obtaining mechanistic information.

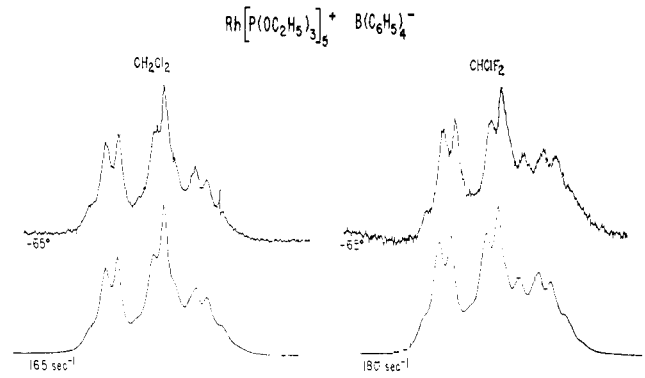

Figure 11. A comparison of the Fourier model $^{31}P\{^1H\}$ nmr spectra of $Rh[P(OC_2H_5)_3]_5^+B(C_6H_5)_4^-$ in CH_2Cl_2 and $CHClF_2$ at −65°. The spectra in the bottom row are simulated using permutational set A and the parameters $\delta_{AB} = 9.74$ ppm exchange rate = 180 sec^{-1} in $CHClF_2$, $\delta_{AB} = 8.37$ ppm exchange rate = 160 sec^{-1} in CH_2Cl_2. The coupling constants were not varied and are the same as given in the text.

F. The Temperature-Dependent Proton Decoupled ^{31}P Nmr Spectra of Other $RhL_5^+X^-$ Complexes

(1) $Rh[P(OC_2H_5)_3]_5^+B(C_6H_5)_4^-$. Figure 10 shows the temperature dependence of the proton noise decoupled Fourier mode ^{31}P nmr spectrum assigned to $Rh[P(OC_2H_5)_3]_5^+B(C_6H_5)_4^-$. The barrier to rearrangement is markedly higher than that in $Rh[P(OCH_3)_3]_5^+B(C_6H_5)_4^-$ and essentially all of the line-shape changes can be observed in CH_2Cl_2 and acetone as solvents. The spectra, and hence the exchange rates, are almost identical at all temperatures showing that the barriers are the same in the two environments. Additional studies were carried out in $CHClF_2$. Here the high-temperature limit cannot be reached, but the useful temperature range in all three solvents does overlap so that direct spectral comparisons can be made. The exchange rate in all three solvents at any given temperature is almost the same. Figure 11 compares the spectra obtained in CH_2Cl_2 and $CHClF_2$ at −65°, together with spectra simulated using the permutational mechanism A. The two spectra were run under the same conditions except that a 1,2-dibromotetrafluoroethane capillary was used to provide a lock for the solution in CH_2Cl_2, whereas the solvent was used without a capillary in the $CHClF_2$ solution. The exchange rates of 180 sec^{-1} in $CHClF_2$ and 160 sec^{-1} in CH_2Cl_2 are not considered to be significantly different. The

difference in appearance between the spectra in Figure 11 does not arise from the difference in exchange rates but is due mainly to a difference in the chemical shift separation between the two types of phosphorus environment (9.74 ppm in $CHClF_2$, 8.37 ppm in CH_2Cl_2). The free energy of activation for the exchange process is ~9.9 kcal mol^{-1} at −65° in all three solvents. At −65° the rate of exchange was low enough for the line shapes to still be sensitive to the chemical shift difference for the two types of ^{31}P environment (Figure 11). Both the exchange rate and the chemical shift difference were varied until a best visual fit was obtained between the observed and calculated spectra. This procedure was also employed for other $RhL_5^+X^-$ complexes. The high-resolution nmr parameters for a solution of $Rh[P(OC_2H_5)_3]_5^+B(C_6H_5)_4^-$ in $CHClF_2$ are J_{AX} = 143 Hz, J_{BX} = 205 Hz, J_{AB} = 68 Hz, and δ_{AB} = 19.7 ppm (with the resonances for the axial phosphorus nuclei upfield) at −125°.

(2) $Rh[P(O\text{-}n\text{-}C_4H_9)_3]_5^+B(C_6H_5)_4^-$. The low-temperature limit proton noise decoupled ^{31}P nmr spectrum assigned to this complex can be accurately fitted using an A_2B_3X model with the parameters $|J_{AX}|$ = 142 Hz, $|J_{BX}|$ = 205 Hz, $|J_{AB}|$ = 70 Hz, and δ_{AB} = 11.94 ppm in $CHClF_2$ at −113°. The resonances assigned to the axial phosphorus nuclei again lie to high field. The line widths in this spectrum are somewhat larger than those observed for the $^{31}P\{^1H\}$ spectra of the other $RhL_5^+B(C_6H_5)_4^-$ complexes. This could arise from a long rotational correlation time for $Rh[P(O\text{-}n\text{-}C_4H_9)_3]_5^+$. The effective volume of this cation in solution may be quite large because of solvent molecules "trapped" between the 15 $OCH_2CH_2CH_2CH_3$ groups. It is also possible that broadening could arise from the superposition of spectra for molecules with different conformations of the ligand alkyl chains, with exchange between the conformations occurring at a rate comparable to the nmr time scale. A line-shape analysis for this complex gives an exchange rate of 105 sec^{-1} at −45° ($\Delta G^{\ddagger}$ = 11.1 kcal/mol^{-1} at −45°). Permutational mechanism A was assumed in the simulation.

(3) $Rh[P(OCH_2)_3CC_2H_5]_5^+B(C_6H_5)_4^-$. The low-temperature limit proton noise decoupled ^{31}P nmr spectrum for this molecule consists of an A_2B_3X pattern consistent with the D_{3h} structure shown in Figure 2. The high-resolution nmr parameters for a solution of this complex in $CHClF_2$ at −137° are J_{AB} = 69.5 Hz, J_{AX} = 140 Hz, J_{BX} = 208 Hz, and δ_{AB} = 10.68 ppm with the resonances assigned to the axial sites *downfield*. The temperature dependence of the spectrum is very similar to that shown for $Rh[P(OCH_3)_3]_5^+B(C_6H_5)_4^-$ in Figures 3–6 and for $Rh[P(OC_2H_5)_3]_5^+B(C_6H_5)_4^-$ in Figure 10. From a complete density matrix line-shape analysis we obtain the result that the exchange rate at −113° is 18 sec^{-1}. The free energy of activation calculated from this result is $\Delta G^{\ddagger}$ = 8.2 kcal mol^{-1} at −113°. In contrast to $Rh[P(OCH_3)_3]_5^+B(C_6H_5)_4^-$, there is essentially *no temperature dependence of the chemical shift separation* for the two phosphorus environments in 15% CH_2Cl_2–85% $CHClF_2$ solution over the temperature range −160 to −100°. A similar insensitivity of shift separation to temperature variation is found for the analogous complex $Rh[P(OCH_2)_3CCH_3]_5^+B(C_6H_5)_4^-$ discussed below, all other complexes studied in this work showing large shift variations. Since ligands involving the $P(OCH_2)_3C$ function are both conformationally more rigid and sterically less bulky than those in the complexes exhibiting the shift variations, the results tend to support the hypothesis that ligand–ligand interactions are responsible for the temperature dependence of the chemical shift difference.

(4) $Rh[P(OCH_2)_3CCH_3]_5^+B(C_6H_5)_4^-$. The low-temperature limit A_2B_3X pattern assigned to the proton noise decoupled ^{31}P nmr spectrum of this complex is almost indistinguishable from the spectrum of $Rh[P(OCH_2)_3CC_2H_5]_5^+B(C_6H_5)_4^-$. The nmr parameters in 15% CH_2Cl_2–85% $CHClF_2$ at −130° are J_{AB} = 69.5 Hz, J_{AX} = 140 Hz, J_{BX} = 208 Hz, and δ_{AB} = 10.7 ppm with the resonances for the axial phosphorus nuclei lying to *low field*. As stated above, the chemical shift separation is temperature independent. The line-shape analysis for this complex gives an exchange rate of 21 sec^{-1} at −120° ($\Delta G^{\ddagger}$ = 7.8 kcal mol^{-1} at −120°).

Conclusion

Stereochemical rigidity has been investigated in a series of complexes of the form $RhL_5^+X^-$ where L is a phosphite and X^- represents a variety of noncoordinating anions using ^1H, ^{13}C, and ^{31}P nmr. The ^1H noise decoupled ^{13}P spectra show that the barrier to intramolecular exchange increases with increasing ligand size. Studies for L = $P(OCH_3)_3$ as a function of concentration and for different anions show that the barrier height is a property of the cation alone and that ion pairing is not an important factor in the exchange process.

A complete density matrix line-shape calculation has been carried out for the A_2B_3X spin system in $Rh[P(OCH_3)_3]_5^+B(C_6H_5)_4^-$. The results show that the intramolecular exchange proceeds by simultaneous exchange of the axial ligands with two of the equatorial ligands in the D_{3h} cation.

There are an infinity of possible physical processes consistent with this observation (including the Berry[6] and turnstile mechanisms[9]). A more detailed discussion of the different proposed physical motions will be presented when data are available for a large body of ML_5 complexes. Processes involving single axial–equatorial exchanges are, however, rigorously excluded.

Acknowledgments. We would like to thank Mr. M. A. Cushing for preparing some of the $RhL_5^+X^-$ complexes and Messrs. G. Watunya and J. M. White for obtaining some of the nmr spectra.

Appendix

Two Useful Approximations for Nmr Line-Shape Analysis. The complete density matrix line-shape analysis for $Rh[P(OCH_3)_3]_5^+B(C_6H_5)_4^-$ using an A_2B_3X model for the proton noise decoupled ^{31}P nmr spectrum is one of the most complex yet attempted. Using the numerical factoring procedure described in ref 13 and neglecting all transitions of zero intensity (see below), the largest complex non-Hermitian matrix which must be diagonalized has dimensions 30 × 30. For the $H_2Fe[P(OC_2H_5)_3]_4$ case,[13] a complete line-shape analysis of the $AA'XX'Y^2$ spectrum required the diagonalization of complex non-Hermitian matrices with dimensions up to 20 × 20 for the hydride region proton nmr spectrum and up to 28 × 28 for the undecoupled ^{31}P

spectrum (ignoring the ligand protons). While the analysis of these spectra was possible without resorting to any approximations, it is important to establish the reliability and utility (in terms of computer storage requirements and time requirements) of approximate methods which may be applied to even more complex spin systems. Two such approximate methods are discussed using the spectral parameters for $Rh[P(OCH_3)_3]_5^+B(C_6H_5)_4^-$.

A. Omission of Lines of Low Intensity from the Calculation.[15] Under the conditions of slow passage, high temperature, and weak radio frequency field, the absorption intensity at angular frequency ω is given by

$$I(\omega) = -\mathrm{Re}[\mathbf{M}^-(\chi + \mathbf{R} - i\mathcal{L}_0(\omega))^{-1}\mathbf{M}^-] \quad (1A)$$

where $\chi = \Sigma_i\chi_i$ is the exchange operator in Liouville space, $\mathbf{R}$ is the relaxation matrix and $\mathcal{L}_0(\omega)$ is the Liouville operator corresponding to the high-resolution nmr Hamiltonian $\mathcal{H}_0$. $\mathbf{M}^- = \Sigma_i\gamma_i\mathbf{I}_i^-$ where $\mathbf{I}_i^-$ is a vector in Liouville space containing the elements of the spin lowering operator for the ith nucleus in ordinary Hilbert space.

In the omission of lines of low intensity approximation all elements of $\mathbf{M}^-$ with values below a particular chosen value are eliminated together with the corresponding rows and columns of $(\mathbf{R} + \chi - i\mathcal{L}_0(\omega))^{-1}$ in eq 1. In this way the dimension of the matrices which must be diagonalized is reduced. It should be noted that this process can only be carried out in the basis in which the Hamiltonian $\mathcal{H}_0$ and the Liouville operator $\mathcal{L}_0 = 2\pi(\mathcal{H}_0 \otimes E^* - E \otimes \mathcal{H}_0^*)$ are diagonal since only in this basis is there a 1:1 correspondence between the observed transitions and the off-diagonal density matrix elements. Figure 12 (rows A–G) compares the calculated results for an A_2B_3X spectrum[16] in which all lines with intensity less than 0.01 have been eliminated with those in which all lines are included. Permutational mechanism A was used in these simulations. The omission of the low-intensity lines reduces the dimension of the largest matrix which must be diagonalized from 30 × 30 to 22 × 22 with a concomitant reduction in core storage requirements by a factor of $(22/30)^2 = 0.54$ and diagonalization time by a factor of $\sim(22/30)^3 = 0.39$ for this stage of the calculation. As can be seen from Figure 12A–G the agreement between the two sets of calculated spectra is near perfect except at very high exchange rates. In Figure 12H the diagonal elements of χ have been altered to satisfy the condition

$$-\sum_j{}'\chi_{ij}\mathbf{M}_j^- = \chi_{ii}\mathbf{M}_i^- \quad (2A)$$

after the low-intensity lines have been omitted. The prime on the summation symbol in the above equation indicates that the term $\chi_{ii}\mathbf{M}_i^-$ is excluded. The condition given in eq 2A is satisfied before the lines of low intensity are eliminated and eq 2A can be regarded as a detailed balance condition for the transverse magnetization. This modification seems to considerably improve the fit obtained at high exchange rates (compare 12A and 12H). The approximation has also been tested on the hydride region ^1H nmr spectrum of $H_2Fe[P(OC_2H_5)_3]_4$[13] with satisfactory results.

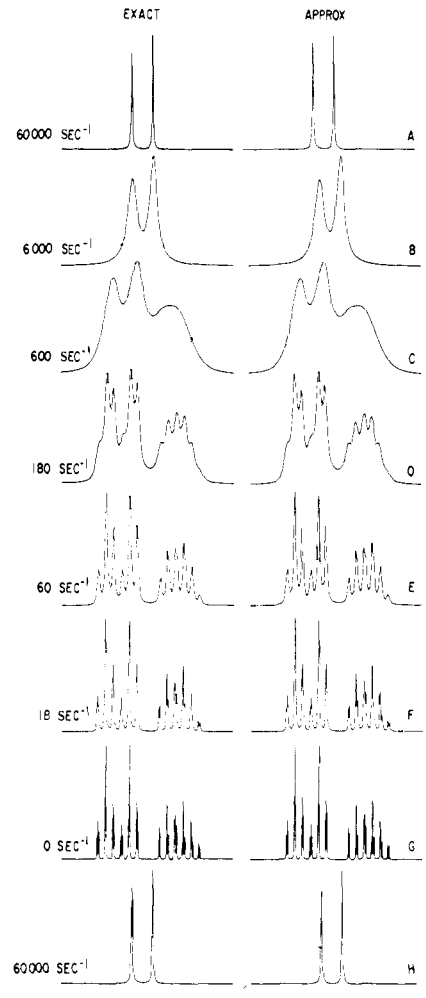

Figure 12. Comparison of the line shapes for an exchanging A_2B_3X system using an exact density matrix calculation (left-hand side) and an approximation in which all lines of intensity less than 0.01 are omitted from the calculation. Basic mechanism A was used for these simulations.

The line omission approximation is not satisfactory in all cases and often is adequate only at low and intermediate exchange rates (it is always useful at higher rates than the approximation discussed in the next section of this appendix). In some cases the calculated fast-exchange limit spectrum does not even qualitatively resemble the true spectrum. The approximation appears to be most reliable in those cases where all the factored blocks of $(\chi + \mathbf{R} - i\mathcal{L}_0(\omega))$ give a single line in the fast-exchange limit. This is true for both of the basic permutational sets in the case of proton noise decoupled ^{31}P nmr spectra of the ML_5 complexes investigated in this work and for all the basic sets which give a high-temperature limit binomial quintet for the hydride region ^1H nmr spectra of the iron dihydrides of the type H_2ML_4. In these cases reliable mechanistic and rate information can be obtained if the line omission approximation is used carefully.

This approximation must be used with caution and the high-temperature limit spectrum should be checked against that calculated directly from the high-temperature limit effective high-resolution nmr Hamiltonian. If the high-temperature limit spectrum is correct using

(15) The approximation discussed in this section has been suggested independently by Professor G. M. Whitesides (G. M. Whitesides, private communication).

(16) The nmr parameters used in this simulation are $J_{AB} = 67.5$ Hz, $\delta_{AB} = 527$ Hz, $J_{AX} = 207$ Hz, and $J_{BX} = 142$ Hz.

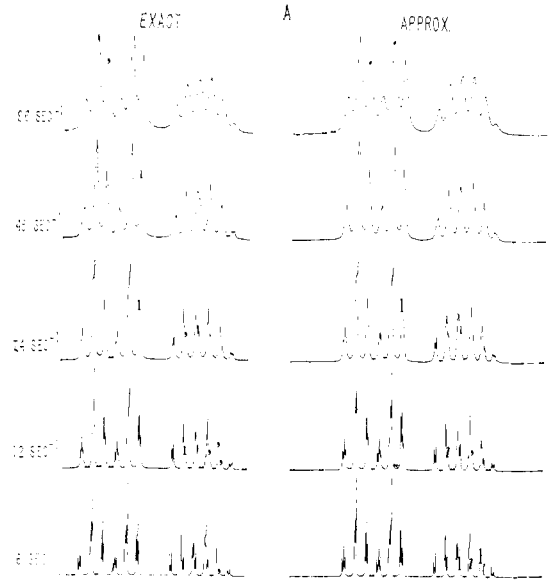

Figure 13. Comparison between the exact calculated line shapes for an exchanging A_2B_3X spin system and the line shapes calculated from the diagonal elements only of $(\mathbf{R} + \mathbf{\chi} - i\mathcal{L}_o(\omega))$. Basic set A was used in these calculations.

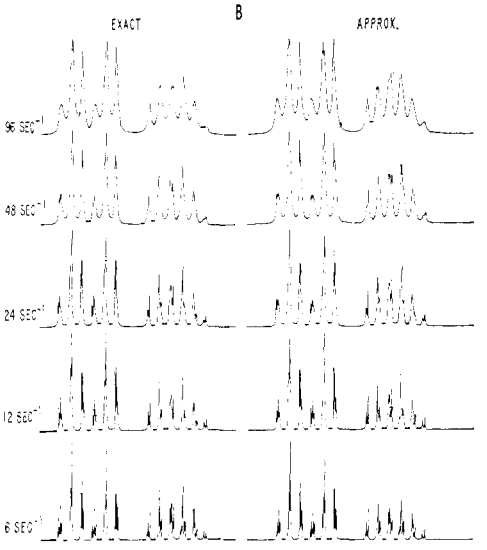

Figure 14. Comparison between the exact calculated line shapes for an exchanging A_2B_3X system and the line shapes calculated from the diagonal elements only of $(\mathbf{R} + \mathbf{\chi} - i\mathcal{L}_o(\omega))$. Basic set B was used in these simulations.

this approximation, the approximation will probably be reliable at all exchange rates. In any event this approximate method may be used in conjunction with that described in section B (below), and where these two approximations agree, they may be used with confidence.

The high-resolution nmr Hamiltonian for a D_{3h} ML_5 system is invariant to any permutation of the equatorial ligands among themselves or to a permutation of the axial ligands, *i.e.*, the high-resolution nmr Hamiltonian is invariant to the operators of the group $S_3 \otimes S_2$ (isomorphic with D_{3h}). Since D_{3h} is not an Abelian group the results given in Appendix II of ref 13 do not apply and $[\mathbf{R} + \mathbf{\chi} - i\mathcal{L}_o(\omega)]$ has matrix elements connecting both forbidden and allowed transitions. If these transitions of zero intensity are included in the calculation, the dimension of the largest complex non-Hermitian matrix which must be diagonalized becomes too large for our programs to handle (dimension greater than 48 × 48) on the Univac 1108 with 64 K of core. As a result the zero intensity transitions were omitted from the calculations in the same manner that lines of low intensity are omitted in the approximation described above. However, the omission of these lines of zero intensity does not seem to be an approximation. The validity of this procedure was tested in two ways: (A) for the smaller matrices in the calculations, their contribution to the overall line shape was invariant to omission or inclusion of the zero intensity lines connected by $[\mathbf{\chi} + \mathbf{R} - i\mathcal{L}_o(\omega)]$, (B) the calculations were repeated using the model

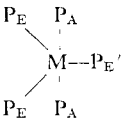

with $\delta_{E'E} = 0.01$ Hz and $J_{AE'} - J_{AE} = 0.01$ Hz. The point group of the molecule and the group of the high-resolution nmr Hamiltonian are now Abelian. Despite the increase in the number of allowed transitions on reducing the symmetry from D_{3h} to C_{2v}, the dimension of the largest non-Hermitian matrix which must be diagonalized is now less than 48 × 48. The line shapes calculated using this model are indistinguishable from those calculated from the D_{3h} model with omission of lines of zero intensity when compared visually. The numerical results are, of course, slightly different.

B. Neglect of the Off-Diagonal Elements of $(\mathbf{R} + \mathbf{\chi} - i\mathcal{L}_o(\omega))$ in the Basis in Which $\mathcal{L}_o$ is Diagonal. By setting the off-diagonal elements of $(\mathbf{\chi} + \mathbf{R} - i\mathcal{L}_o(\omega))$ equal to zero, one can avoid the necessity of diagonalizing this complex non-Hermitian matrix. To a first-order approximation the positions and line widths of the individual lines in the spectra are given by the diagonal elements of $(\mathbf{\chi} + \mathbf{R} - i\mathcal{L}_o(\omega))$. This first-order approximation provides an adequate description of the spectrum provided that the effects of **R** and **X** on the line widths are sufficiently small that the lines in the spectrum are well resolved (*i.e.*, provided that the T_2 values are large and the exchange rate is slow). The approximation begins to break down when $\mathbf{A}_{ij}$ is of comparable magnitude to $\mathbf{A}_{ii} - \mathbf{A}_{jj}$ where $\mathbf{A} = (\mathbf{\chi} + \mathbf{R} - i\mathcal{L}_o(\omega))$. Since only the diagonal elements of **A** need be computed and since no complex non-Hermitian matrix diagonalization step is required, the reduction in computer time and core storage requirements may be dramatic. In most cases if the high-resolution nmr Hamiltonian can be diagonalized, then the line shapes can also be calculated using this approximation and the calculation of the nmr line shapes for, say, an ABCDEFG problem would be feasible. Since the most unambiguous distinction between different possible permutational mechanisms may in many cases be obtained from the slow-exchange region where the spectrum is just starting to broaden, the approximation can be very useful.

In Figures 13 and 14 the simulated spectra for an A_2B_3X spin system are compared using the complete density matrix method and using the approximation discussed above for basic mechanisms A and B. In

both cases the slow-exchange limit nmr parameters are held constant at the values J_{AB} = 67.5 Hz, δ_{AB} = 527 Hz, J_{AX} = 207 Hz, and J_{BX} = 142 Hz used in the previous section.

In this case the spectra using the exact method and the first-order approximation are almost indistinguishable for exchange rates up to 100 sec^{-1} for both basic set A (Figure 13) and basic set B (Figure 14). In an experimental situation, of course, the first-order approximation could only be relied on at those rates where the lines being used to obtain rate or mechanistic information remained well resolved, *i.e.*, up to about 25 sec^{-1} for the outer doublets associated with the axial ligands.

A comparison of Figures 13 and 14 with the observed spectrum shown in Figure 3 indicates that in this case reliable mechanistic information could be obtained from this approximation. In general, the better the resolution the more useful this "first-order" approximation will become.

Caution must be exercised in applying this approximation to systems with degenerate transitions.

Addition of a Coordinated Nucleophile to a Free Carbonyl Center. The Formation of Acetylacetonatobis(ethylenediamine)cobalt(III) Ion

D. A. Buckingham, J. MacB. Harrowfield, and A. M. Sargeson*

Contribution from the Research School of Chemistry, Australian National University, Canberra, A.C.T. 2600, Australia.
Received May 15, 1973

Abstract: The mechanism of formation of $[Co(en)_2acac]^{2+}$ from *cis*-$[Co(en)_2(OH_2)OH]^{2+}$ and -$[Co(en)_2(OH)_2]^{+}$ and acetylacetone (acacH) is shown to occur by addition of the two coordinated oxygens to the two carbonyl centers of acetylacetone. Retention of configuration at Co(III) is implied and observed. Some reactant complex isomerization to *trans*-$[Co(en)_2(OH_2)OH]^{2+}$ is detected along with $[Co(en)_2acac]^{2+}$ formation and reconversion to the cis form leads to formation of more $[Co(en)_2acac]^{2+}$ (racemate) as a secondary process. The isomerization and racemization of the hydroxoaqua species are also examined. From consideration of the limited data available on the oxygen exchange between acetylacetone and water, an estimate of the residual nucleophilicity of OH^- when coordinated to Co(III) is made.

The reaction between *cis*-$[Co(en)_2(OH_2)OH]^{2+}$ (en = 1,2-diaminoethane) and 2,4-pentanedione (acetylacetone) to form $[Co(en)_2acac]^{2+}$ was first described by Werner.[1] Its rapidity has more recently been noted by Boucher and Bailar,[2] though some forcing is required to drive the reaction to completion.[3] While the diaqua and dihydroxo complexes have been studied rather thoroughly with respect to isomerization[4,5] and oxygen exchange[5] in water, rather less is known about the hydroxoaqua species. They are certainly more reactive than their protonated and deprotonated counterparts, but only one ^{18}O exchange measurement has been made where the hydroxoaqua concentration was reasonable[5] and the isomerization reactions also have only been studied in a desultory way.[5-7] This paper now examines the reaction between the hydroxoaqua ion and acetylacetone and also the interconversion of the cis and trans isomers and the racemization of the cis ion.

Experimental Section

Spectrophotometric measurements were made on Cary 14 and 16 instruments and rotations were determined for a 1-dm cell on a Perkin-Elmer P22 spectropolarimeter. Readings of pH were taken on a Radiometer pH meter with TTA_3 electrode assembly, and mass spectral measurements were made on AEI MS902 and Atlas M86 instruments.

Acetylacetone (Fluka, puriss) was dried over anhydrous Na_2SO_4 and fractionally distilled immediately prior to use. 2,4,6-Collidine was fractionally distilled prior to the preparation of buffers. All other chemicals were of analytical reagent grade. Cation exchange experiments were conducted with Bio-Rad Analytical Grade Dowex 50WX2 (200-400 mesh) resin.

Synthesis. *cis*-$[Co(en)_2(OH_2)OH](ClO_4)_2$ was prepared by adjusting the pH of an ice-cold solution of *cis*-$[Co(en)_2(OH_2)_2]^{3+}$ to a value between 7 and 8 and allowing the complex to crystallize, essentially the procedure described by Kruse and Taube.[5] The trans isomer was obtained by recrystallizing this material from hot water. It was also prepared simply by adding 1 mol of $LiOH \cdot H_2O$ to a concentrated solution of *cis*-$[Co(en)_2(OH_2)_2]^{3+}$ at room temperature. Solutions of *cis*-$[Co(en)_2(OH_2)_2](ClO_4)_3$ were prepared by dissolving *cis*-$[Co(en)_2CO_3]ClO_4$ in a slight excess (5%) of $HClO_4$ (5 *M*) and heating until all CO_2 had been displaced.

Anal. Calcd for $CoC_4H_{19}N_4Cl_2O$: Co, 14.3; C, 11.6; H, 4.6; N, 13.6; Cl, 17.2. Found: (cis) Co, 14.3; C, 11.7; H, 4.8; N, 13.6; Cl, 17.2; (trans) Co, 14.2; C, 11.8; H, 4.6; N, 13.5; Cl, 17.1.

$[Co(en)_2acac]I_2 \cdot H_2O$. Finely ground *cis*-$[Co(en)_2(OH_2)OH](ClO_4)_2$ (2.0 g) was added to a solution of 2,4-pentanedione (0.5 g) in water (10 ml). The mixture was stirred for 15 min, then filtered and treated with excess NaI. Red crystals formed immediately and, after 15 min of cooling on ice, were collected and washed with ethanol and ether, yield 2.2 g (83%). The complex was recrystallized from water.

Anal. Calcd for $CoC_9H_{27}N_4O_3I_2$: Co, 10.71; C, 19.65; H, 4.58; N, 10.19; I, 46.14. Found: Co, 11.17; C, 19.64; H, 4.59; N, 10.17; I, 46.17.

Kinetics. All rate measurements were made at 25°. Measurements of the isomerization rates of the $[Co(en)_2(OH_2)OH]^{2+}$ ions at other temperatures have been made previously.[6]

(1) A. Werner and S. Matissen, *Helv. Chim. Acta*, **1**, 78 (1917).
(2) L. J. Boucher and J. C. Bailar, Jr., *Inorg. Chem.*, **3**, 589 (1964).
(3) I. K. Reid and A. M. Sargeson, *Inorg. Syn.*, **9**, 167 (1960).
(4) J. Bjerrum and S. E. Rasmussen, *Acta Chem. Scand.*, **6**, 1265 (1952).
(5) W. Kruse and H. Taube, *J. Amer. Chem. Soc.*, **83**, 1280 (1961).
(6) M. E. Baldwin, S. C. Chan, and M. L. Tobe, *J. Chem. Soc.*, 4637 (1961).
(7) R. D. Gillard, *J. Chem. Soc. A*, 1945 (1968).